Journal of Inorganic Biochemistry 131 (2014) 1–7

Contents lists available at ScienceDirect

Journal of Inorganic Biochemistry

journal homepage: www.elsevier.com/locate/jinorgbio

Immobilization of the enzyme GpdQ on magnetite nanoparticles for organophosphate pesticide bioremediation

Lena J. Daumann [a], James A. Larrabee [b], David Ollis [c], Gerhard Schenk [a], Lawrence R. Gahan [a,*]

[a] School of Chemistry and Molecular Biosciences, The University of Queensland, Brisbane QLD 4072, Australia
[b] Department of Chemistry and Biochemistry, Middlebury College, Middlebury VT 05753, USA
[c] Research School of Chemistry, Australian National University, Canberra 0200, Australia

ARTICLE INFO

Article history:
Received 14 June 2013
Received in revised form 8 October 2013
Accepted 8 October 2013
Available online 16 October 2013

Keywords:
Metalloenzyme
Magnetite nanoparticles
Organophosphate pesticide
Bioremediation

ABSTRACT

Annually thousands of people die or suffer from organophosphate (pesticide) poisoning. In order to remove these toxic compounds from the environment, the use of enzymes as bioremediators has been proposed. We report here a Ser127Ala mutant based on the enzyme glycerophosphodiesterase (GpdQ) from *Enterobacter aerogenes*. The mutant, with improved metal binding abilities, has been immobilized using glutaraldehyde on PAMAM dendrimer-modified magnetite nanoparticles. The immobilized system was characterized using elemental analysis as well as infrared, transmission electron and X-ray photoelectron spectroscopies. The amount of GpdQ that was immobilized with the optimized procedure was 1.488 nmol per g MNP. A kinetic assay has been designed to evaluate the activity of the system towards organophosphoester substrates. The specific activity towards BPNPP directly after immobilization was 3.55 μmol mg^{-1} min^{-1}, after one week 3.39 μmol mg^{-1} min^{-1} and after 120 days 3.36 μmol mg^{-1} min^{-1}, demonstrating that the immobilized enzyme was active for multiple cycles and could be stored on the nanoparticles for a prolonged period.

© 2013 Elsevier Inc. All rights reserved.

1. Introduction

It is estimated that thousands of people die or suffer from severe organophosphate (OP) pesticide poisoning *per annum* [1]. The use of pesticides has distinct benefits but there are risks to people and the environment, especially in developing countries. How to eliminate these compounds from the environment to avoid contamination of waterways and deleterious effects on human health has been raised [1–4]. As well as pesticides, OPs have also been used as nerve agents, for example sarin and VX (Chart 1) [3]. The hydrolysis of OPs, whether as agricultural agents or as weapons, to less harmful compounds is thus an important aspect for environmental decontamination. The phosphate ester bond is prone to cleavage, mostly by hydrolysis, but photolytic degradation by sunlight is also possible [5]. Biological pathways such as bioremediation have also attracted recent attention [6].

The glycerophosphodiesterase GpdQ from *Enterobacter aerogenes* was first purified by Gerlt and co-workers [7] and is believed to be the first known phosphoesterase capable of hydrolysing stable alkyl diesters like dimethyl phosphate and diethyl phosphate [8,9]. GpdQ is a dinuclear metallohydrolase (Chart 1) with a highly stable hexameric structure, able to degrade di- and monoester substrates, making it a versatile and thus ideal candidate for applications in bioremediation [8–11]. It has also attracted attention for its ability to degrade an analogue of EA 2192, a highly toxic degradation product from the VX nerve gas [8]. Although the catalytic rates of wild-type GpdQ for OP triesters are significantly lower than those of triesterases such as the OP-degrading enzyme A (OpdA) from *Agrobacterium radiobacter* or OP-hydrolase (OPH) from *Pseudomonas diminuta*, GpdQ functions over a large pH range (between pH 3 to pH 11) [12,13]. Furthermore, recent directed evolution experiments have indicated that the catalytic activity of GpdQ can be significantly enhanced by the introduction of a small number of mutations [14].

The most recent crystal structure of GpdQ at high resolution (1.9 Å) illustrates an extensive hydrogen bonding network in the active site, the latter composed of two distinct metal binding sites (labelled as the α and β-sites, Chart 1) [15]. The α-site features four amino acid side chains, two aspartates (Asp50, Asp8) and two histidines (His10, His197), whereas the metal in the β-site is coordinated by two histidines (His156, His195), one aspartate (Asp50) and one asparagine (Asn80). The crystal structure also suggests the presence of a terminal H_2O bound to the α-metal and a bridging water/hydroxide molecule. The active site is surrounded by an extensive hydrogen bond network connecting it with the second coordination sphere [15]. Although the metal ion content of GpdQ in vivo is currently unknown, it was initially proposed, on the basis of spectroscopic and crystallographic results, that the native metal ion composition was Fe(II)Zn(II). The reactivity of apo-GpdQ can, however, be readily reconstituted with Co(II), Mn(II), Fe(II), Zn(II) and even Cd(II) [16,17]. As Co(II) serves as an excellent spectroscopic probe, the Co(II)Co(II) derivative is the best studied metal derivative. From magnetic circular dichroism (MCD) spectroscopy studies of Co(II)-

* Corresponding author. Tel.: +61 7 336 53844.
E-mail address: gahan@uq.edu.au (L.R. Gahan).

0162-0134/$ – see front matter © 2013 Elsevier Inc. All rights reserved.
http://dx.doi.org/10.1016/j.jinorgbio.2013.10.007

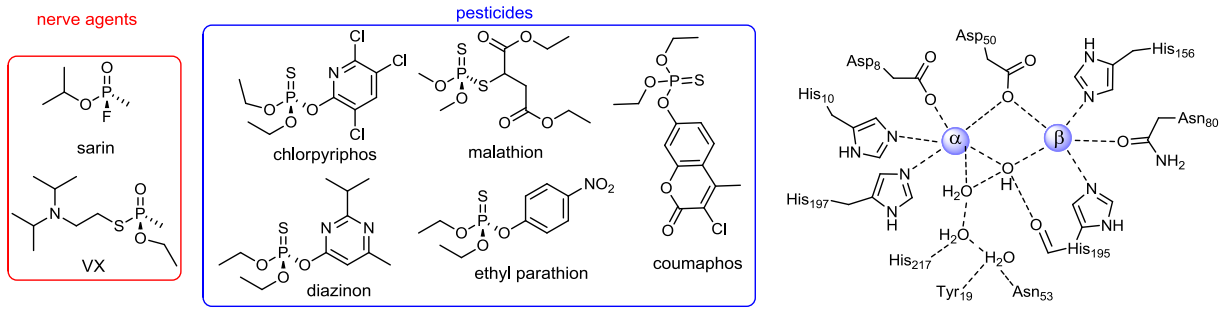


Chart 1. Examples of organophosphates used as nerve agents and pesticides, active site of GpdQ.

substituted GpdQ it is known that GpdQ exists as a mononuclear resting state enzyme with only the α-site being occupied by a metal ion [10]. It could also be shown that the catalytically relevant dinuclear Co(II)Co(II) metal centre in GpdQ is only formed in the presence of a substrate analogue [13]. The metal ion affinity of the β-site can be increased by changing the Asn80 residue (Chart 1; Note: the term ligand is not used since not all residues are ligands) to an aspartate, resulting in a fully occupied dinuclear centre after the addition of two equivalents of Co(II) to the apo-enzyme, even in the absence of substrate [10]. Thus the combined directed evolution and site directed mutagenesis studies have demonstrated that GpdQ is amenable to modifications to increase both its catalytic efficiency and stability [14]. The challenge now is to deliver an active and stable enzyme in a manner suitable for use in aquatic media and to make the system robust and recyclable.

GpdQ has been subjected previously to mutagenesis studies in an attempt to enhance both catalytic properties and metal ion binding [14]. In order to evolve GpdQ activity towards the non-physiological substrate bis(4-nitrophenyl)phosphate (BPNPP) a range of mutants were obtained by directed evolution [14]. Some mutants exhibited increased activity towards BPNPP and, in some, the hexameric structure of the wild-type enzyme was disrupted [14]. Mutants contained, on average, three amino acid substitutions; one mutation that was often present was a Ser127Ala, a residue located in the second coordination sphere directly next to Asn80. Previous studies have shown that the structural flexibility of the Asn80 residue plays a crucial role in regulating Co(II) binding to the β-site [12]. In terms of designing a potential bioremediator it is important to note that Asn80 facilitates coordination flexibility, a property that enables wild-type GpdQ to optimize its catalytic efficiency [15]. However, this flexibility also reduces the affinity of the β-site for a metal ion, leading to an inactive enzyme in the resting state. The substitution of the asparagine ligand by an aspartate increased the affinity of the β-site for metal ions, but also reduced catalytic efficiency greatly. In order to utilise GpdQ effectively a mutant is required that maintains a high affinity for both metal ions in the resting state without compromising catalytic efficiency. Since Ser127 forms a hydrogen bonding interaction with Asn80, and since this residue also lines the substrate binding pocket, it was speculated that its replacement by an alanine may disrupt this H-bond and thus increase the metal ion affinity of the β-site without greatly affecting catalysis.

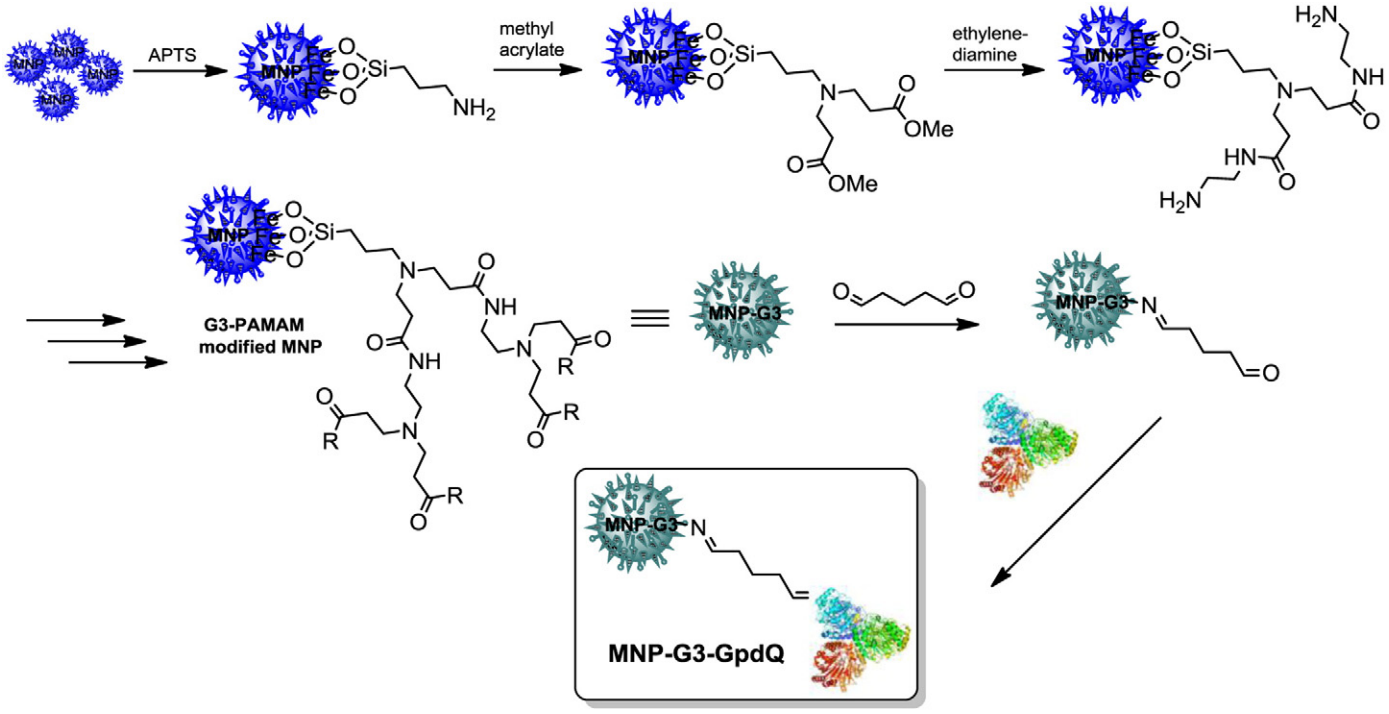
In an approach to utilise enzymes to degrade pesticides, recombinant OPH on the surface of *Escherichia coli* cells was packed in a bioreactor on glass beads [18]. A similar approach used *E. coli* cells with OPH on the surface, immobilized on silica beads [19] or nylon [20]. In 2005 a group reported the immobilization of OPH on a cellulose matrix via an attached cellulose binding domain for the degradation of coumaphos [21]. Ginet et al. functionalized lipid-coated magnetic nanoparticles with a phosphohydrolase for the degradation of the pesticide ethyl-paraoxon; the kinetic properties were comparable to the free enzyme [22]. Dendrimer-modified and plain magnetite nanoparticles (MNPs) have been extensively studied for their potential application in environmental decontamination, medicine and biology [23–26]. For example, MNPs coated with receptor proteins or other functional molecules have found application in imaging and therapy [27–29]. Grüttner et al. reported MNPs functionalized with chelating groups on the surface to bind lanthanides and actinides in order to remove radionuclides from nuclear wastes [25]. Magnetically assisted processes have been reported to purify water [26] and MNPs have been proven useful in protein immobilization and purification and DNA extraction [24,30]. The main advantage of magnetite nanoparticles is that they can be easily recovered from the reaction media by magnetic separation.

In this study we present the synthesis of a GpdQ system (Scheme 1) immobilized on magnetite nanoparticles that have been functionalized with a G3-PAMAM dendrimer. The potential use of these systems for water treatment purposes is discussed.

2. Experimental

2.1. General methods and materials

Elemental microanalyses (C, H, N, S) were performed with a Carlo Erba Elemental Analyser model NA1500 by Mr. George Blazak at the University of Queensland. FT-Infrared Spectroscopy was carried out with a Perkin Elmer FT-IR Spectrometer SPECTRUM 2000 with a Smiths DuraSamplIR II ATR diamond window. Transmission electron microscopy (TEM) was conducted at the Centre of Microscopy and Microanalysis, The University of Queensland, together with Dr. Graeme Auchterlonie. Nanoparticles were taken up in water and sonicated for 10 min after which time the suspension was transferred onto a carbon grid. A JEOL JEM2100 LaB_6 STEM analytical transmission electron microscope with an EM-21010/21020 single tilt holder was used to analyse the samples after the water had evaporated. X-ray photoelectron spectroscopy (XPS) was conducted with Dr. Barry Wood at the Centre for Microscopy and Microanalysis, The University of Queensland, with a Kratos Axis Ultra photoelectron spectrometer which uses Al K_α (1253.6 eV) X-rays. The software Casa XPS was used for data processing [31]. Chemical reagents were obtained from Aldrich Chemical Company and were used without further purification. Expression and purification of Ser127Ala GpdQ were conducted following previously published methods [16,17]. Preparation of the apo-enzyme for the MCD measurements was undertaken using a known protocol [16]. Samples of the Ser127Ala mutant of GpdQ (0.71 mM) were generated for the MCD studies by adding two equivalents of Co(II) to the apo-protein ($CoCl_2 \cdot 6H_2O$, 14 mM in 50 mM HEPES pH 7.0). The mixture was dissolved in a 60%/40% (v/v) mixture of glycerol/buffer (50 mM 4-(2-hydroxyethyl)-1-piperazineethanesulfonic acid (HEPES), pH 7.0) and loaded in a 0.62 cm path length nickel-plated copper sample cell with quartz



Scheme 1. Synthesis of GpdQ-functionalized magnetite nanoparticles.

windows. K_2HPO_4 was added (140 mM, in 50 mM HEPES pH 7). The MCD system used has a JASCO J815 spectropolarimeter and an Oxford Instruments SM4000 cryostat/magnet. Data were collected at 7.0 T and 1.4 K. Each spectrum was corrected for any natural CD by subtracting the zero-field spectrum of the sample. The resultant spectra were fitted to the minimum number of Gaussian peaks to achieve a satisfactory composite spectrum using the GRAMS AI software [32]. Phosphatase activity measurements were conducted using a Varian Cary50 Bio UV/vis spectrophotometer with a Peltier temperature controller and 10-mm quartz cuvettes.

2.2. Synthesis of nanoparticles and enzyme immobilization

2.2.1. Synthesis of G3-PAMAM dendrimer functionalized magnetite nanoparticles (G3-MNPs)

The magnetite nanoparticles were synthesized after modification of a previously published procedure [24,33]. Solutions of ferric chloride (1.15 g in 50 mL degassed water) and ferrous sulphate (0.69 g, in 50 mL degassed water) were combined under nitrogen and 1.5 M ammonia solution was added drop wise with vigorous stirring. As the pH reached 9, the black precipitated magnetite was collected with a magnet and washed with water (5 × 50 mL) and ethanol (2 × 50 mL). The MNPs were dispersed in ethanol to give a 5 wt.% suspension. The G3-PAMAM modified MNPs (G3-MNPs) were synthesized as follows: Magnetite stock solution (100 mL) was sonicated for 30 min and diluted with ethanol (300 mL) in a two-necked flask equipped with a reflux condenser and a pressure equalised dropping funnel. 3-Aminopropyltrimethoxysilane (APTS, 20 mL) was added over 7 h at 60 °C and the nanoparticles were subsequently washed with methanol (3 × 50 mL) by magnetic separation and dried in vacuo. 1.16 g of APTS modified magnetite nanoparticles (APTS-MNPs) was dispersed in methanol (100 mL) and methylacrylate (40 mL) was added. After sonication for 5 min the mixture was stirred overnight at room temperature and washed with methanol (5 × 20 mL). Ethylenediamine (8 mL) and methanol (10 mL) were added and stirred at 50 °C for 5 h. This step was repeated twice with increased amounts of methylacrylate (60 and 80 mL) and ethylenediamine (12 and 20 mL) and the final product was washed with methanol (3 × 50 mL) and water (3 × 50 mL).

MNPs: FT-IR spectroscopy (ν, cm^{-1}) 560 (m, Fe – O str). Microanalysis Fe_3O_4: found C 0.24, H 0.35, N 0.05, S 0.75% (slight sulphur contamination due to sulphate residues).

APTS-MNPs: FT-IR spectroscopy (ν, cm^{-1}) 2949.1, 2866 (w, C – H str); 1014.7 (m, Si – O str); 569 (m, Fe – O str). Microanalysis found C 1.69, H 0.64, N 0.47, S 0.69% (sulphur contamination due to sulphate residues).

G3-MNPs: FT-IR spectroscopy (ν, cm^{-1}) 3314.2 (b, N – H); 2668.4 (w, C – H str); 1624.6, 1551.4 (m, $C{=}O_{Amide}$); 1017.2 (m, Si – O str); 714.5 (w, CH_2); 560 (m, Fe – O str). Microanalysis found C 3.53, H 0.75, N 1.44, S 0.00%.

2.2.2. Functionalizing G3-MNPs with glutaraldehyde and immobilization of Ser127Ala mutant

G3-MNPs (150 mg) were suspended in glutaraldehyde (25%, 20 mL) and the mixture sonicated for 1 h. After 12 h standing, the nanoparticles were separated from glutaraldehyde and washed with TRIS buffer pH 8 (5 × 15 mL). G3-MNP-glutaraldehyde was used in the next step without further purification for the GpdQ immobilization. The G3-MNP (50 mg) functionalized with glutaraldehyde was added to a GpdQ stock solution (0.17 mM, 2 mL, 50 mM HEPES, pH 8) and the mixture was incubated over 24 h at 4 °C. After this time a significant amount of enzyme was bound to the nanoparticles via amide formation between the lysine residues of the enzyme and the pendant aldehydes on the particles. The amount of enzyme immobilized was determined by the decrease in absorbance at 280 nm of the supernatant solution; $A_{280,\ T\ =\ 0} = 0.0772$, $A_{280,\ T\ =\ 24\ h} = 0.0589$. After a thorough washing process (5 × 1.5 mL 50 mM TRIS, pH 8) the GpdQ-nanoparticles were suspended in 0.5 mL buffer (50 mM TRIS pH 8) and stored at 4 °C until further use. The degree of immobilization was calculated to be 1.48 nmol/g based on the decrease in absorbance of the supernatant enzyme solution at 280 nm.

2.3. Activity measurements of immobilized enzyme

To test whether the immobilized enzyme was active towards organophosphates an experimental setup was designed, mimicking water filtration conditions. The nanoparticles were embedded between two layers of sand in a Pasteur pipette and were held in place with a conventional magnet. The bottom of the column was connected with a small tube to a flow through UV/vis cuvette. A buffered solution (50 mM TRIS, pH 8) of the organophosphate substrate BPNPP (5.63 mM) was circled through the column and UV–vis cell with a peristaltic pump at a flow rate of 1.40 mL/min for 3 h. The hydrolysis of the substrate was monitored by the formation of the nitrophenolate ion at 405 nm. After cycling the BPNPP solution through the column for 3 h, the column was detached from the system and washed (3 × 2 mL) with buffer solution and stored at 4 °C under the same buffer as used for the kinetic experiments. The amount of GpdQ that was immobilized with the optimized procedure was 1.488 nmol per g MNP. The specific activity directly after immobilization was 3.55 μmol mg^{-1} min^{-1}, after one week 3.39 μmol mg^{-1} min^{-1} and after 120 days 3.36 μmol mg^{-1} min^{-1} (when using a 5.63 mM solution of BPNPP).

3. Results and discussion

MCD was employed to visualize the effects of the Ser127Ala mutation on Co(II) binding in the presence and absence of a substrate mimic (phosphate). Two equivalents of Co(II) were added to the apo-enzyme solution (50 mM HEPES, pH 7.0) to which glycerol had been added as glassing agent. The resulting MCD spectrum is shown in Fig. 1. In addition to the expected transition from Co(II) bound to the 6-coordinate α-site (~500 nm), a band of 5-coordinate Co(II) was also observed around 580 nm [15]. A noticeable increase in the population of the β-site in the absence of phosphate in the Ser127Ala mutant was observed; this is more obvious when comparing it to the spectrum of wt-GpdQ where two equivalents of added Co(II) only resulted in one spectral feature at 500 nm [15]. In the presence of phosphate both mutant and wild type GpdQ have similar Co(II) populations of α- and β-sites, respectively. Integration of the spectrum indicates that in Ser127Ala mutant GpdQ 40% of the enzyme sample already has a catalytically active dinuclear Co(II)Co(II) site. Importantly, the catalytic parameters are slightly improved by this mutation [16]. On this basis the Ser127Ala mutant was chosen for the immobilization studies since it is expected to maintain considerable catalytic activity even in a metal ion deprived environment. In addition, activity measurements for the freshly purified enzyme mutant, and after it has been stored for one year at 4 °C, showed that the activity remained the same.

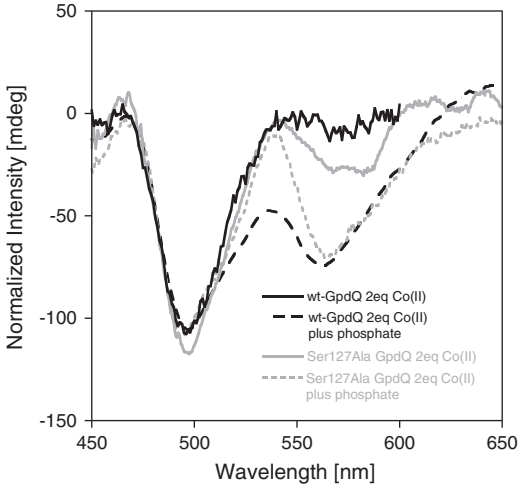


Fig. 1. MCD spectra of the Ser127Ala mutant after adding two equivalents Co(II) in the presence and absence of phosphate. For comparative reasons the spectra of Co(II) wt-GpdQ are also shown. In all samples the six-coordinate site, giving rise the band near 500 nm, is saturated and thus the spectra (that were collected on samples that had different concentrations of protein) were normalized to this band to illustrate the varying degrees of Co(II) occupancy in the five-coordinate site, which gives rise to the bands near 560 nm [15].

3.1. Immobilization of the Ser127Ala mutant of GpdQ

Generation 3 (G3) PAMAM dendrimer modified magnetite nanoparticles were synthesized after a modification of previously published methods [23,24]. The G3-MNP, after functionalization with glutaraldehyde, was added to a Ser127Ala GpdQ mutant stock solution and after 5 days at 4 °C the nanoparticles were washed thoroughly with buffer to remove any unbound enzyme [34]. After this time a sufficient amount of enzyme was bound to the nanoparticles via amide formation between the lysine residues of the enzyme and the pendant aldehydes on the particles. This was confirmed by the decrease of absorbance at 280 nm of the supernatant. The degree of immobilization fluctuated depending on how long the nanoparticles had been stirred with glutaraldehyde previously and also the ratio of nanoparticles to enzyme. G3-MNP-GpdQ was stored suspended in a small amount of buffer and at 4 °C at all times, The kinetic experiments were conducted with nanoparticles where a total of 1.48 nmol GpdQ per g MNP had been immobilized.

3.2. Characterization of the nanoparticles

The nanoparticles were characterized employing a number of techniques. Infrared analysis of unsubstituted magnetite nanoparticles showed a band from Fe–O at 560 cm^{-1}. Once APTS was attached to the surface, additional C–H stretches at 2949 cm^{-1} and 2866 cm^{-1} and Si–O stretch at 1015 cm^{-1} were found. In the G3-MNP, N–H and C═O_{Amide} stretches were apparent (3314 and 1625, 1551 cm^{-1}). Elemental analyses were conducted to confirm the successful synthesis of the G3-MNP and to monitor the increasing nitrogen content during dendrimer immobilization. An overview is shown in Table S1. Some sulphur contamination is apparent (presumably from the ferrous sulphate used in the MNP synthesis); this contamination is washed out during the repeated sonication/washing processes during subsequent PAMAM dendrimer modification. A small amount of sulphur is found after GpdQ had been immobilized, which may be due to cysteine residues and traces of sulphate bound to the enzyme.

At different stages of functionalization the nanoparticles were analysed with X-ray photoelectron spectroscopy. Figs. 2a and S2 shows the survey spectrum of the magnetite nanoparticles reflecting the degree of functionalization with the PAMAM dendrimer. In general, the survey spectrum of G3-MNP-GpdQ displays more noise (Fig. 2a), attributed to the multitude of trace elements bound to the enzyme and thus appear in the XPS spectrum. Figs. 2a and S2 show that after the immobilization of the G3-PAMAM dendrimer, the surface analysis shows nitrogen and small amount of silicon present [35]. The silicon is proposed to be present from silicon oils used in the vacuum system of the XPS instrument [36]. A closer examination of the G3-MNP spectrum reveals that the core material is indeed Fe_3O_4 [37,38]. Two types of iron are found in this sample corresponding to the two environments of Fe(II)/(III) in Fe_3O_4 (Fig. 2b) [37,39]. The binding energies of the Fe 2p peak (~710.0 eV) and also the O1s peak ~529.5 eV strongly point to Fe_3O_4 [37,39]. Moreover, oxygen peaks in two different environments could be assigned to species containing C═O and C–O [35,40]. Similar to the oxygen 1s peak in the spectrum of G3-MNP (Fig. S3a), the O1s peak in G3-MNP-GpdQ can be Gaussian deconvoluted into four separate peaks (Fig. 2c). The peak at highest energy (~533.3 eV) may be attributed to C═O, following C–O (~532.2 eV), an unidentified O1s (~531.1 eV) and oxygen in the form

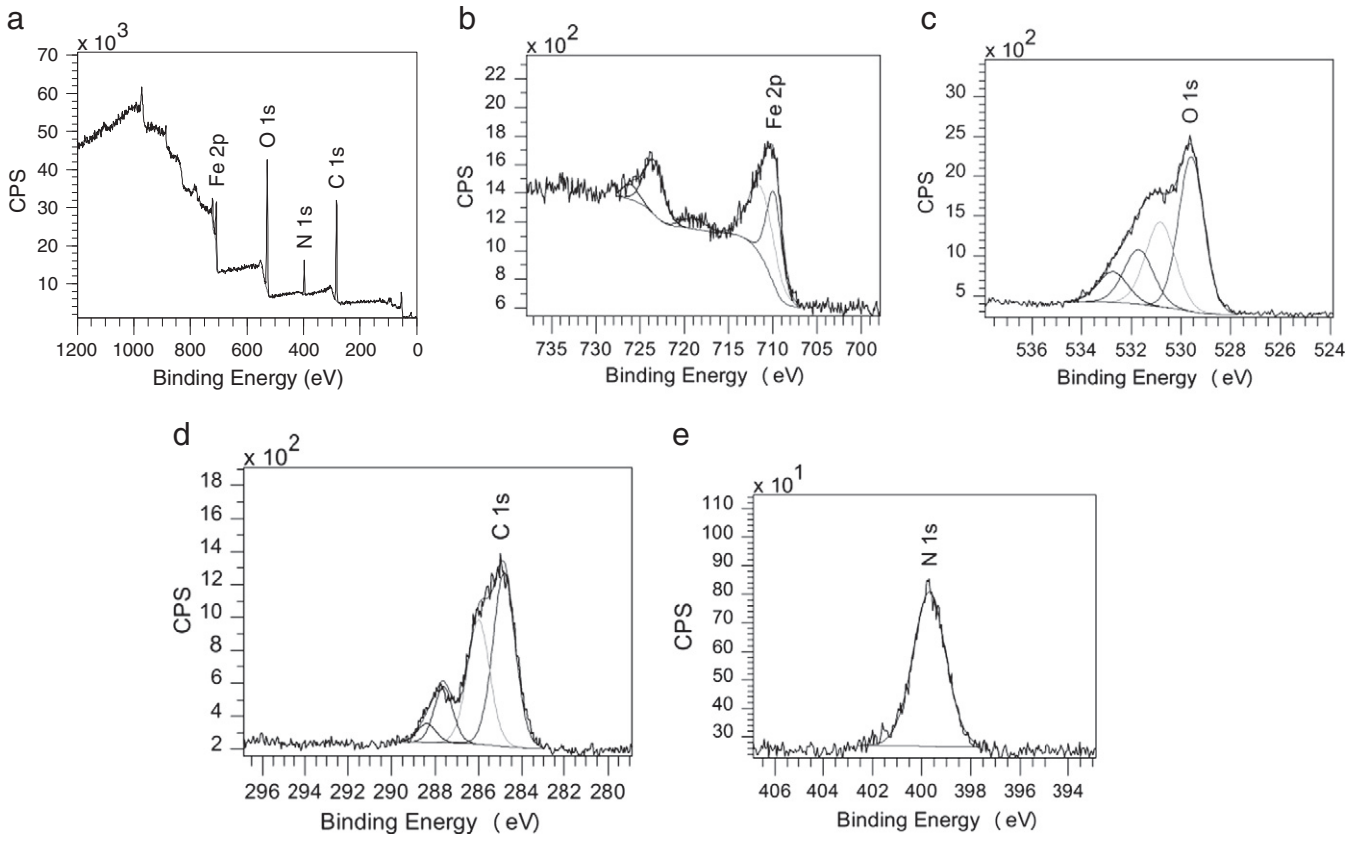


Fig. 2. Survey (a) and Gaussian deconvoluted Fe 2p (b), O 1s (c), C 1s (d) and N 1s (e) spectra of G3-MNP-GpdQ.

of (Fe) oxide (~529.8 eV) [35,40]. The survey spectrum demonstrates that the elements present on the surface are mainly iron, oxygen, nitrogen and carbon (Fig. 2a) [35]. While the O1s and C1s peaks could be resolved into multiple species the assignment for nitrogen is less clear (Fig. 2c, d and e).

Transmission electron microscopy was conducted with the nanoparticles to investigate the size, shape and clustering behaviour. Prior to the measurements ca ~20 mg of the nanoparticles was diluted with 1 mL of water and sonicated for 30 min. The suspension was then applied onto 600 mesh carbon grids and dried in air for several minutes. Particle sizes from 5 to 20 nm are observed (Fig. 3a) confirming the 'nanoparticle nature' of the magnetite. Fig. 3a and b suggests that the MNPs are spherical. Moiré fringes are also observed from an interference pattern by the atomic layers of the iron oxide (Fig. 3c) [41]. Moreover, the magnetic behaviour is demonstrated by the clustering of the nanoparticles as demonstrated in Fig. 3b. The TEM sample preparation of the immobilized enzyme was difficult since only water could be used to suspend the nanoparticles (usually a more volatile solvent is favoured) and prolonged sonication times were avoided since this could cause the enzyme to detach from the nanoparticles. Resulting TEM images (Fig. 4) demonstrate that the nanoparticles are surrounded by organic matter (the enzyme). Analysis of the diffraction patterns of the darker spots inside the organic matter confirmed them to be Fe_3O_4.

3.3. Use of immobilized GpdQ in filter systems

To test whether the immobilized enzyme was active towards OPs (i.e. BPNPP in this study) an experimental setup that mimics water filtration conditions was designed. The nanoparticles were embedded

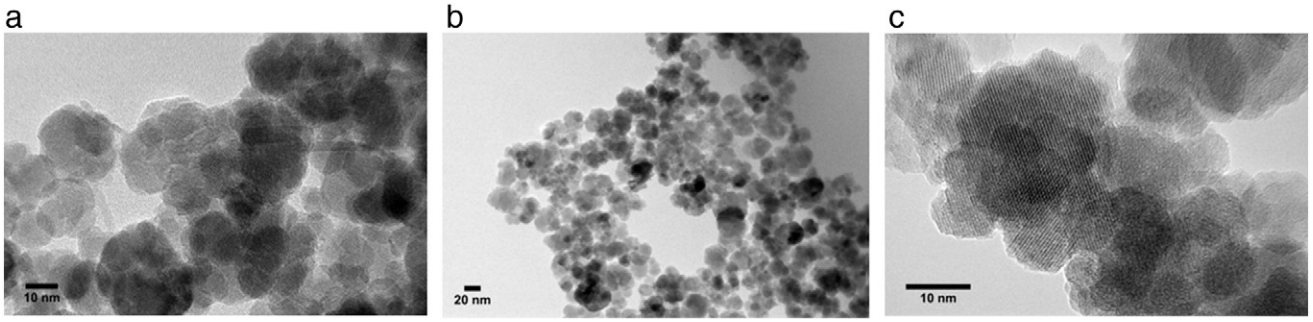


Fig. 3. TEM images of plain magnetite nanoparticles at two magnifications (50 K (a) and 200 K (b)) and (c) TEM image of magnetite nanoparticles with APTS anchored at the surface at a magnification of 400 K.

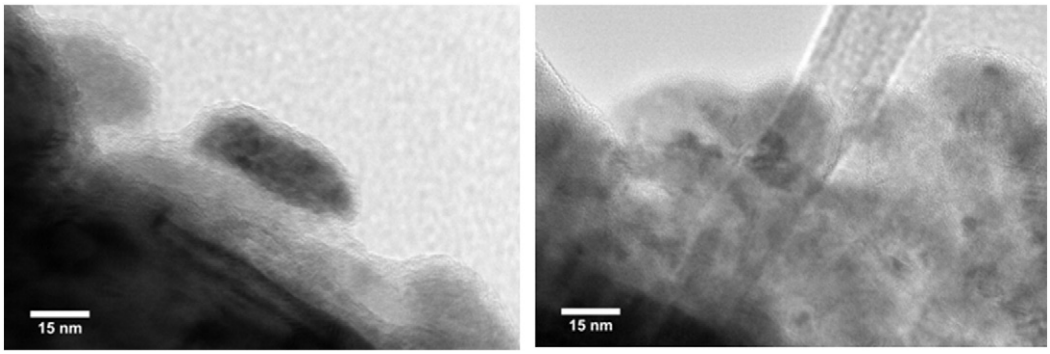


Fig. 4. TEM images of GpdQ immobilized on G3-MNP.

between two layers of sand in a Pasteur pipette (Figs. S3 and S4). A buffered solution of organophosphate substrate (BPNPP, 5.63 mM) was circulated through the column and the hydrolysis of the substrate was monitored by the formation of the nitrophenolate ion at 405 nm (the use of the phosphate ester BPNPP and its resulting highly coloured hydrolysis product permits ready analysis of the progress of the reaction) [16]. After periods of 7 and 120 days the experiment was repeated. The activity towards BPNPP was shown to be largely unaffected by the storage (Table 1). After 120 days an experiment with different concentrations of BPNPP was also conducted.

4. Conclusion

The Ser127Ala mutant of GpdQ was attached to G3-PAMAM dendrimer modified magnetite nanoparticles using glutaraldehyde. The MNPs were characterized with IR, microanalysis, XPS and TEM at different stages of functionalization. TEM confirmed the nanoparticle character and XPS affirmed that the nanoparticles were made of Fe_3O_4 and also provided insight into the elemental composition of the surface after PAMAM generation. Kinetic experiments with the immobilized GpdQ mutant showed that the enzyme was active on the nanoparticles and that it could be stored over a prolonged time in the immobilized form without loss of activity. This system has the potential, upon further development, to be of potential use in the bioremediation of organophosphate contaminated waterways.

Acknowledgements

This work was funded by a grant from the Australian Research Council (DP0986613). LJD was funded by IPRS and UQ graduate school scholarships. The M.G. & R.A. Plowman Scholarship in Inorganic Chemistry (School of Chemistry and Molecular Biosciences, The University of Queensland), and Royal Australian Chemical Institute (RACI) grants awarded to LJD assisted with visits to Middlebury College for experiments reported in this paper and are gratefully acknowledged. JAL wishes to acknowledge the National Science Foundation (USA) for financial support from grants CHE 0848433, CHE 1303852, and CHE 0820965 (MCD instrument).

Table 1
Specific activities of immobilized GpdQ.

	T = 0 d	T = 7 d	T = 120 d
Specific activity when using 5.63 mM BPNPP [μmol mg^{-1} min^{-1}]	3.55	3.39	3.36
Specific activity when using 2.81 mM BPNPP [μmol mg^{-1} min^{-1}]	–	–	2.95
Specific activity when using 1.41 mM BPNPP [μmol mg^{-1} min^{-1}]	–	–	1.97

Appendix A. Supplementary data

Supplementary data to this article can be found online at http://dx.doi.org/10.1016/j.jinorgbio.2013.10.007.

References

[1] J. Jeyaratnam, World Health Stat. Q. 43 (1990) 139–144.
[2] I. Horne, M. Selleck, M.R. Williams, K.M. Weir, J.G. Oakeshott, R.J. Russell, T.D. Sutherland, C.W. Coppin, Clin. Exp. Pharmacol. Physiol. 31 (2004) 817–821.
[3] J. Newmark, Neurologist 13 (2007) 20–32.
[4] S.W. Wiener, R.S. Hoffman, J. Intensive Care Med. 19 (2004) 22–37.
[5] T.M. Sakellarides, M.G. Siskos, T.A. Albanis, Int. J. Environ. Anal. Chem. 83 (2003) 33–50.
[6] C. Scott, G. Pandey, C.J. Hartley, C.J. Jackson, M.J. Cheesman, M.C. Taylor, R. Pandey, J.L. Khurana, M. Teese, C.W. Coppin, K.M. Weir, R.K. Jain, R. Lal, R.J. Russell, J.G. Oakeshott, Ind. J. Microbiol. 48 (2008) 65–79.
[7] J.A. Gerlt, G.J.R. Whitman, J. Biol. Chem. 250 (1975) 5053–5058.
[8] E. Ghanem, Y. Li, C. Xu, F.M. Raushel, Biochemistry 46 (2007) 9032–9040.
[9] C.J. Jackson, P.D. Carr, J.W. Liu, S.J. Watt, J.L. Beck, D.L. Ollis, J. Mol. Biol. 367 (2007) 1047–1062.
[10] C.J. Jackson, K.S. Hadler, P.D. Carr, A.J. Oakley, S. Yip, G. Schenk, D.L. Ollis, Acta Crystallogr. F 64 (2008) 681–685.
[11] C.J. Jackson, P.D. Carr, H.K. Kim, J.W. Liu, D.L. Ollis, Acta Crystallogr., Sect. F: Struct. Biol. Cryst. Commun. 62 (2006) 659–661.
[12] K.S. Hadler, N. Mitić, S.H. Yip, L.R. Gahan, D.L. Ollis, G. Schenk, J.A. Larrabee, Inorg. Chem. 49 (2010) 2727–2734.
[13] K.S. Hadler, N. Mitić, F. Ely, G.R. Hanson, L.R. Gahan, J.A. Larrabee, D.L. Ollis, G. Schenk, J. Am. Chem. Soc. 131 (2009) 11900–11908.
[14] S.H.-C. Yip, J.-L. Foo, G. Schenk, L.R. Gahan, P.D. Carr, D.L. Ollis, Protein Eng. Des. Sel. (2011) 1–12.
[15] K.S. Hadler, E.A. Tanifum, S.H. Yip, N. Mitić, L.W. Guddat, C.J. Jackson, L.R. Gahan, K. Nguyen, P.D. Carr, D.L. Ollis, A.C. Hengge, J.A. Larrabee, G. Schenk, J. Am. Chem. Soc. 130 (2008) 14129–14138.
[16] L.J. Daumann, B.Y. McCarthy, K.S. Hadler, T.P. Murray, L.R. Gahan, J.A. Larrabee, D.L. Ollis, G. Schenk, Biochim. Biophys. Acta, Proteins Proteomics 1834 (2013) 425–432.
[17] R.E. Mirams, S.J. Smith, K.S. Hadler, D.L. Ollis, G. Schenk, L.R. Gahan, J. Biol. Inorg. Chem. 13 (2008) 1065–1072.
[18] A.H. Mansee, W. Chen, A. Mulchandani, Biotechnol. Bioprocess Eng. 5 (2000) 436–440.
[19] D.M. Munnecke, Biotechnol. Bioeng. 21 (1979) 2247–2261.
[20] S. Caldwell, F. Raushel, Appl. Biochem. Biotechnol. 31 (1991) 59–73.
[21] W. Chen, A. Mulchandani, A.H. Mansee, J. Ind. Microbiol. Biotechnol. 32 (2005) 554–560.
[22] N. Ginet, R. Pardoux, G. Adryanczyk, D. Garcia, C. Brutesco, D. Pignol, PLoS One 6 (2011) e21442.
[23] F. Gao, B.-F. Pan, W.-M. Zheng, L.-M. Ao, H.-C. Gu, J. Magn. Magn. Mater. 293 (2005) 48–54.
[24] B.-F. Pan, F. Gao, H.-C. Gu, J. Colloid Interface Sci. 284 (2005) 1–6.
[25] C. Grüttner, V. Böhmer, A. Casnati, J.-F. Dozol, D.N. Reinhoudt, M.M. Reinoso-Garcia, S. Rudershausen, J. Teller, R. Ungaro, W. Verboom, P. Wang, J. Magn. Magn. Mater. 293 (2005) 559–566.
[26] R.D. Ambashta, M. Sillanpää, J. Hazard. Mater. 180 (2010) 38–49.
[27] J. Jayapaul, S. Arns, W. Lederle, T. Lammers, P. Comba, J. Gätjens, F. Kiessling, Biomaterials 33 (2012) 8822–8829.
[28] J.A. Barreto, W. O'Malley, M. Kubeil, B. Graham, H. Stephan, L. Spiccia, Adv. Mater. 23 (2011) H18–H40(Weinheim, Ger.).
[29] Y.-w. Jun, J.-H. Lee, J. Cheon, Angew. Chem. Int. Ed. Engl. 47 (2008) 5122–5135.
[30] B. Yoza, A. Arakaki, T. Matsunaga, J. Biotechnol. 101 (2003) 219–228.
[31] C.S. Ltd, CasaXPS: Processing Software for XPS, AES SIMS and More, 2009.

[32] T. Scientific, Grams/AI 9.0 Software.
[33] R.S. Molday, United States Canadian Patents and Development Limited (CA) 4452773 (1984).
[34] L.S. Wong, F. Khan, J. Micklefield, Chem. Rev. 109 (2009) 4025–4053(Washington, DC, U. S.).
[35] C.D. Wanger, W.M. Riggs, L.E. Davis, J.F. Moulder, G.E. Muilenberg, Handbook of X-ray Photoelectron Spectroscopy, Perkin-Elmer Corp., Physical Electronics Division, Minnesota USA, 1979.
[36] G.L. Weissler, R.W. Carlson, Vacuum Physics and Technology, Academic Press, New York, 1979.
[37] A. Baykal, M.S. Toprak, Z. Durmus, M. Senel, H. Sozeri, A. Demir, J. Supercond. Novel Magn. 25 (2012) 1541–1549.
[38] NIST, X-ray photoelectron spectroscopy database, version 4.1, http://srdata.nist.gov/xps/ (Site accessed February 2013).
[39] B.J. Tan, K.J. Klabunde, P.M.A. Sherwood, Chem. Mater. 2 (1990) 186–191.
[40] J.C. Vickerman, Surface Analysis: The Principal Techniques, John Wiley, New York, 1997.
[41] J. Guild, The Interference Systems of Crossed Diffraction Gratings: Theory of Moire Fringes, Clarendon Press, Oxford, 1956.